

In Situ ^{13}C MAS NMR Study of *n*-Hexane Conversion on Pt and Pd Supported on Basic Materials

Part I. Identification of the Main Reaction Pathways and Comparison with Microcatalytic Reactor Tests

Irina I. Ivanova*¹ Anne Pasau-Claerbout,* Michaël Seirvert,* Niels Blom,[†] and Eric G. Derouane*²

**Facultés Universitaires N.-D. de la Paix, Laboratoire de Catalyse, 61 Rue de Bruxelles, B-5000 Namur, Belgium; and* [†]*Haldor Topsøe A/S Research Laboratories, Nymøllevej 55, P.O. Box 213, DK-2800 Lyngby, Denmark*

Received May 3, 1995; revised September 19, 1995; accepted September 29, 1995

n-Hexane conversion was studied *in situ* on Pt and Pd supported on aluminum-stabilized magnesium oxide and Pt on Zeolite KL catalysts (Pt/Mg(Al)O, Pd/Mg(Al)O and Pt/KL) by means of ^{13}C MAS NMR spectroscopy. *n*-Hexane $1\text{-}^{13}\text{C}$ was used as a labelled reactant. Forty NMR lines corresponding to 14 different products were resolved and identified. The NMR line assignments were confirmed by adsorption of model compounds. The NMR results were further quantified and compared with continuous flow microreactor tests. Four parallel reaction pathways were identified under flow conditions: isomerization, cracking, dehydrocyclization, and dehydrogenation. Aromatization occurs via two reaction routes: (1) *n*-hexane dehydrogenation towards hexadienes and hexatrienes, followed by dehydrocyclization; (2) dehydrocyclization of *n*-hexane followed by dehydrogenation of a cyclic intermediate. The former reaction pathway is prevented under NMR batch conditions. High pressures induced in the NMR cells at high reaction temperatures (573, 653 K) shift the reaction equilibrium towards hydrogenation. NMR experiments showed that on Pt catalysts aromatization occurs via a cyclohexane intermediate, whereas on Pd it takes place via methylcyclopentane ring enlargement. © 1996 Academic Press, Inc.

INTRODUCTION

Petroleum light naphtha containing mostly $\text{C}_6\text{--}\text{C}_7$ molecules is an important constituent of motor gasoline. It has a rather low research octane rating of 45–70 (1, 2). The demand for increased octane number stimulates the necessity to convert light straight chain hydrocarbons to branched aliphatic hydrocarbons and aromatics. However, in conventional reforming (2–5), a large part of the $\text{C}_6\text{--}\text{C}_7$

fraction is hydrocracked. Reforming catalysts which favor aromatization consist of Pt supported on nonacidic materials such as KL zeolite (6–14) and aluminum-stabilized magnesium oxide (15–18). An unusually high selectivity to aromatics is observed for Pd supported on Al-stabilized MgO (17–18).

Several explanations are proposed to account for the increased selectivity of noble metal nonacidic supported catalysts. One explanation is that selectivity benefits from the absence of acid-catalyzed hydrocracking and isomerization (14). However, it does not account for the observation of increased activity. The other view points to a significant role of the support on the desired catalytic reaction and can be classified as either a geometric (9, 10, 13, 14) or chemical effect of the support (8, 11, 16–18, 19–23).

Detailed mechanistic information, in particular on the structures of the surface-bound intermediate species, may give a key for a better understanding of the role of both the metal and the support. Thus, *in situ* mechanistic studies performed on well-characterized surfaces of platinum allowed elucidation of the mechanisms of alkane skeletal rearrangements on various crystallographic surfaces (24–27). As to metal catalysts supported on basic materials, no direct *in situ* information on the mechanism of reforming reactions is available as yet.

The potential of the ^{13}C MAS NMR technique for *in situ* studies of catalytic reactions has been demonstrated recently (24–40). It allows one to observe different types of adsorbed species, to infer their chemical state and mobility, to monitor their fate during the course of reaction, to identify reaction intermediates and surface active sites, and to determine approximate reaction rates.

However, the application of this technique for elucidating reaction mechanisms has limitations, especially for catalysts containing a metal component (35). Part of the ^{13}C

¹ On leave from Moscow State University, Russia.

² Present address: Department of Chemistry, The University of Liverpool, P.O. Box 147, Liverpool L69 3BX, U.K.

nuclei which are in close contact with metal particles may not be observed due to susceptibility broadening (32). Moreover, *in situ* NMR experiments are performed in sealed NMR cells (28, 31–34) or rotors (29, 30, 37), which leads to longer than normal contact times. Long contact times favor observation of the most stable products; consequently, the intermediates in consecutive reactions are not necessarily observed (34, 38–40). Since the volume of the NMR cells is rather low (0.5–1 cm³), reactants and products may induce high pressures in the NMR cell, when the reaction requires high temperatures. This can affect reaction kinetics and equilibrium, e.g., the ratio between parallel pathways may change dramatically and may lead to different product distributions (40). Thus, investigation of the relationship of the *in situ* NMR results to those obtained under flow conditions was the first step in our mechanistic study. We have used the conversion of *n*-hexane on Pt/Mg(Al)O, Pd/Mg(Al)O, and Pt/KL as the target reaction.

This paper is the first in a series of papers devoted to the mechanistic study of *n*-hexane 1-¹³C conversion over Pt/Mg(Al)O, Pd/Mg(Al)O, and Pt/KL catalysts. It describes the main reaction pathways observed by the *in situ* MAS NMR technique and the major differences with microcatalytic tests.

EXPERIMENTAL

Materials

Reactants. *n*-Hexane 1-¹³C (99.9% enriched), used as labelled reactant, was obtained from ICON Services Inc. The methylcyclopentane, cyclohexane, 1-hexene, and 1,5-hexadiene used as model compounds were obtained from Aldrich Chemical Company, Fluka Chemika, Janssen Chemica, and Fluka Chemika, respectively.

Catalysts. Stabilized high-area MgO support was prepared by coprecipitation of Mg and Al nitrates in a 5:1 Mg:Al molar ratio in the presence of KOH and K₂CO₃ (41). The resulting hydroxycarbonates (hydrotalcite structure confirmed by X-ray diffraction) were decomposed in air at 873 K for 12 h. The specific surface area of the final stabilized magnesia was 220 m² g⁻¹.

Stabilized magnesia was impregnated with an aqueous solution of Pt(NH₃)₄Cl₂ (Johnson Matthey Specpure) or Pd(NO₃)₂ · xH₂O (Ventron-Agfa), dried, and calcined in air at 650 K for 6 h to yield 1.12 wt.% Pt and 0.78 wt.% Pd catalysts; designated as Pt/Mg(Al)O and Pd/Mg(Al)O, respectively. The calcined material was reduced in a flow of H₂ at 700 K for 2 h.

Zeolite L in the potassium form (Linde) was ion exchanged with aqueous Pt(NH₃)₄Cl₂, washed, dried, calcined, and reduced according to the above procedure for the magnesia sample, to give a final Pt loading of 1.85 wt.%.

The dispersion (*D*) of the metal particles in the catalysts was determined as $D = N_s/N_{\text{tot}}$, where *N_s* corresponds to the fraction of the metal atoms exposed at the surface and *N_{tot}* to the total amount of metal atoms in the catalyst. *N_{tot}* was obtained from chemical analysis and *N_s* from the isotherms of hydrogen adsorption using the following procedure. A sample was first reduced in a flow of H₂ at 700 K for 2 h, evacuated at that temperature for 1 h, and cooled to room temperature in vacuum. The isotherm of hydrogen adsorption was then measured at room temperature (RT) in a standard static volumetric adsorption apparatus. The linear part of the adsorption isotherm was extrapolated to zero pressure to obtain the number of hydrogen atoms associated with the metal surface (both physisorbed and chemisorbed). The catalyst was then evacuated for 0.5 h at RT to remove only physisorbed hydrogen and the back-sorption isotherm was measured. Subtraction of the latter gave the number of H₂ molecules chemisorbed as atoms on the metal particles. Since the stoichiometry of dihydrogen chemisorption is about 1 H per 1 atom of metal (42), the number of chemisorbed H atoms gave the fraction of metal atoms exposed at the surface (*N_s*). The metal dispersions were determined to be of 0.89, 0.63, and 0.93 for Pt/Mg(Al)O, Pt/KL and Pd/Mg(Al)O, respectively. The metal particle sizes calculated from these dispersions were 13, 18, and 11 Å, respectively.

In situ MAS NMR Measurements

In situ ¹³C MAS NMR measurements were carried out on a MSL-400 Bruker spectrometer operating at 100.6 MHz. The spinning rate was 3.8 kHz. Quantitative conditions were achieved using high-power gated proton-decoupling with suppressed NOE effect (5 μs 90° pulse, recycling delay = 4 s). Some non-¹H-decoupled spectra were recorded to identify reaction products and intermediates. Variable-temperature (253–373 K) and cross-polarization (contact time 5 ms) experiments were performed to distinguish between the species with different mobilities. If the given resonance was shifted significantly with respect to data in solution or gaseous phase, the assignment of this signal was verified by the determination of the corresponding chemical shift of the model compound in the adsorbed state.

In situ ¹H MAS NMR measurements were carried out on a MSL-400 Bruker spectrometer operating at 400.13 MHz. A pulse length of 1 μs (90° pulse), a recycling delay of 5 s, and a spinning rate of 3.8 kHz were used.

The NMR cells were prepared using the following procedure. Powdered catalysts (0.15 ± 0.01 g) were packed into NMR tubes (Wilma, 5.6 mm o.d. with constrictions) fitting exactly the double-bearing Bruker zirconia rotors, and evacuated. The catalysts were then reduced prior to the adsorption. For that, H₂ was introduced up to a pressure

of 500 Torr (1 Torr = 133.3 N m⁻²) and temperature was raised to 703 K at a rate of 5 K/min. These conditions were maintained for 4 hours. Then the samples were evacuated to a pressure of 6×10^{-6} Torr and cooled to 298 K. From 1 to 12 mg of *n*-hexane 1-¹³C were dosed gravimetrically and adsorbed onto the catalyst sample in the NMR tube. Quantitative adsorption was ensured by cooling the sample to 77 K. After introduction of the reactant, the NMR cells maintained at 77 K to avoid local overheating were carefully sealed to achieve proper balance and high spinning rates in the MAS NMR probe. Preparation of the samples with adsorbed model compounds was performed in a similar way. Gaseous compounds (propane 2-¹³C) were dosed volumetrically.

The *n*-hexane 1-¹³C reaction was carried out by heating the sealed NMR cells outside the spectrometer. The MAS NMR measurements were performed at lower temperatures (in most cases at 293 K) after the quenching of the sample cells. After collection of the NMR data, NMR cells were returned to reaction conditions. Two different reaction protocols were used. In the first one, the temperature was increased in a stepwise manner, the NMR spectra being recorded at each temperature step. In other experiments the sample was rapidly heated to a final temperature and maintained at this temperature for various durations of time. ¹³C spectra were recorded over the time course of the reaction. The first experimental mode showed more clearly a sequence of products, while the second one facilitated a comparison of reaction kinetics.

Conversion of reactant *n*-hexane 1-¹³C at time *t* ($X_{r,t}$) was determined as,

$$X_{r,t} = (1 - I_{r,t}/I_{r,0}) \cdot 100 [\%],$$

where $I_{r,t}$ corresponds to the integral intensity of the reactant *r* NMR resonance after heating for *t* min and $I_{r,0}$ corresponds to the integral intensity of the reactant *r* NMR resonance in the initial NMR spectrum. The yield of reaction product *p* at time *t* ($Y_{p,t}$) was determined as *n*-hexane 1-¹³C conversion into the product concerned,

$$Y_{p,t} = (I_{p,t}/I_{r,0}) \cdot 100 [\%],$$

where $I_{p,t}$ corresponds to the integral intensity of the product *p* resonance in the NMR spectrum after heating for *t* min. Selectivity to different products ($S_{p,t}$) was determined as a percentage of a product in feed-free products:

$$S_{p,t} = (Y_{p,t}/X_{r,t}) \cdot 100 = I_{p,t}/(I_{r,0} - I_{r,t}) \cdot 100 [\%].$$

Continuous-Flow Microreactor/GC Catalytic Tests

Both the magnesia and zeolite catalysts were tested in a single-flow, quartz, tubular reactor (4 mm i.d.) for the

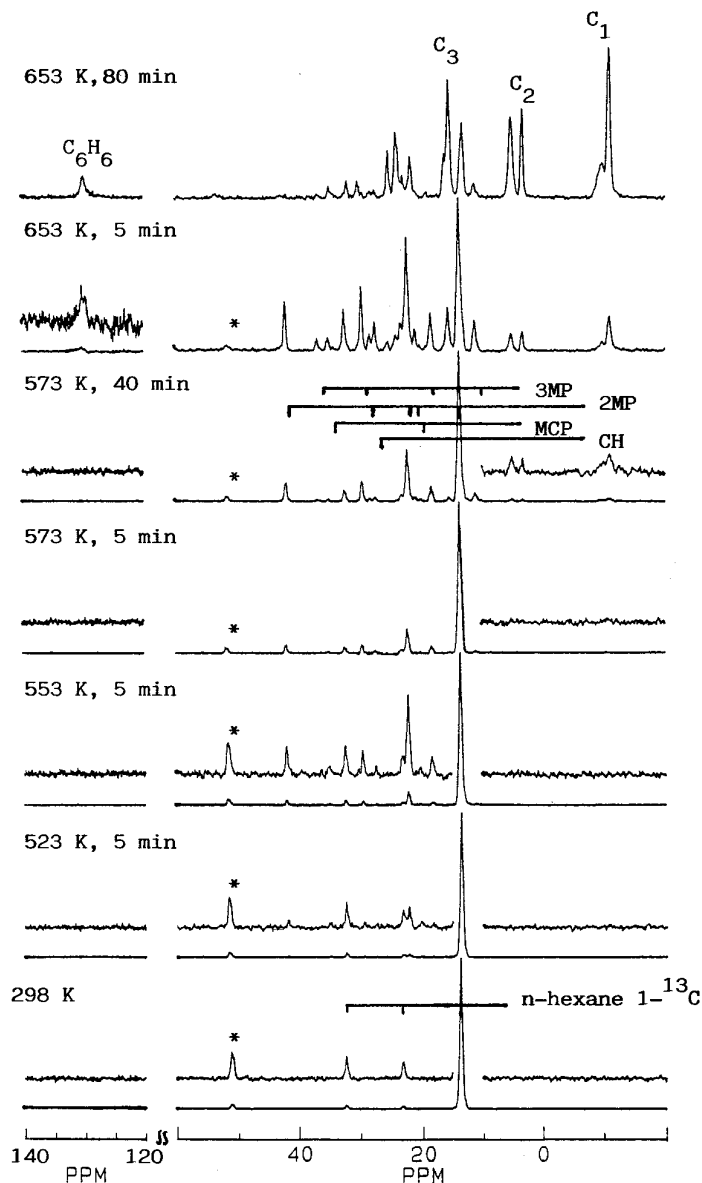


FIG. 1. ¹³C MAS NMR spectra observed before and after reaction of *n*-hexane 1-¹³C over Pt/Mg(Al)O at progressively increasing temperatures. Abbreviations used: 3MP, 3-methylpentane; 2MP, 2-methylpentane; MCP, methylcyclopentane; CH, cyclohexane; C₃, propane; C₂, ethane; C₁, methane. Asterisks denote spinning sidebands.

steady state conversion of *n*-hexane at 750 K and atmospheric total pressure (40 kPa H₂, diluent He) with a ratio of H₂ to hydrocarbon of six. The catalyst powders were pressed without binder into pellets, then crushed and size separated to give catalyst grains between 0.25 and 0.50 mm in diameter. Helium (Air Liquide, 99.99%) and electrolytically generated dihydrogen (Milton Roy) passed through MnO/silica indicators to show the absence of oxygen in the gas streams before mixing and entering a double saturator containing *n*-hexane (Merck, 99.0%) at 273 K. The reactant

TABLE 1

Assignments of the Resonances Observed after Conversion of *n*-Hexane 1-¹³C over Pt/Mg(Al)O, Pt/KL, and Pd/Mg(Al)O Catalysts

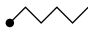



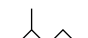

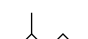


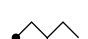
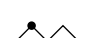
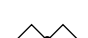
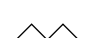


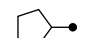
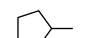
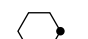
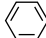
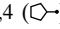

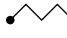
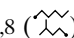
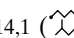
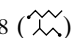

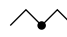
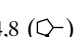
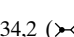
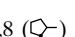

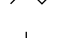

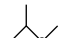
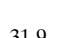
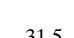


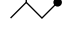
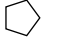
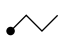


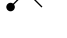
Assignment ^a	Experimental δ (ppm) ^b			Splitting ^c
	Pt/Mg(Al)O	Pt/KL	Pd/Mg(Al)O	
Reactant				
 (13,7 _s)	13,8	14,1	13,8	4
 (22,8 _s)	23,2	23,0	23,3	3
 (31,9 _s)	32,3	32,1	32,4	3
 g	—	11,0	—	(4)
Isomerisation products				
 (22,4 _s)	22,2	22,4	22,3	4
 (27,6 _s)	28,3	28,2	28,2	(2)
 (41,6 _s)	41,8	41,7	41,9	3
 (20,5 _s)	21,0	20,8	20,9	3
 (14,0 _s)	13,8 (⊗⊗)	14,1 (⊗⊗)	13,8 (⊗⊗)	4
 (11,1 _s)	11,0	11,1 (∧)	11,1 (∧)	(4)
 (29,1 _s)	29,5	29,8 (∧)	29,5	(3)
 (36,5 _s)	36,7	—	36,8	2
 (18,4 _s)	18,4	18,5	18,3	(4)
 (19,1 _s)	19,1	19,3	—	(4)
 (33,9 _s)	34,1	34,2 (∧)	—	(2)
Dehydrocyclization products				
 (21,4 _s)	20,3*	—	20,3*	(4)
 (35,8 _s)	34,9* (∧)	—	34,9* (∧)	(3)
 (27,6 _s)	27,4*	27,2	—	3

TABLE 1—Continued

Assignment ^a	Experimental δ (ppm) ^b			Splitting ^c
	Pt/Mg(Al)O	Pt/KL	Pd/Mg(Al)O	
Aromatization products				
 (128,5 _s)	130,3	110–135	129,7	—
Alkylsubstituted benzenes:				
Methyl (15–21) _s	—	—	20,4 ()	
Ethyl (25–30; 15–16) _s	—	—	28,2 ()	
Aromatic carbons (144–125) _s	—	—	125, 139	
Cracking products				
 (13,7 _s)	13,8 ()	14,1 ()	13,8 ()	4
 (22,6 _s)	22,7	22,6	22,8	—
 (34,6 _s)	34,8 ()	34,2 ()	34,8 ()	(3)
 (21,9 _s)	21,7	21,8	21,7	—
 (29,7 _s)	30,2	29,7	—	—
 (31,7 _s)	31,9	31,5	—	—
 (11,4 _s)	11,0 ()	11,0 ()	11,1 ()	(4)
 (25,8 _s)	—	—	26,0	—
 (13,2 _s)	13,2	13,3	13,3	(4)
 (24,9 _s)	25,3	24,8	25,3	(3)
 (24,6 _s)	24,3	24,1	24,1	—
 (23,3 _s)	23,9	23,4	24,0	—
 (16,1 _s ; 15,4 _g)	15,6	15,0	15,5	4
 (16,3 _s ; 16,1 _g)	16,2*	16,5	16,1	4
CH ₃ -CH ₃ (6,5 _s ; 3,2 _g)	3,2; 5,1	3,2; 5,1	3,3; 5,2	4
CH ₄ (-2,3 _s ; -11 _g)	-11,0; -9,7	-10,9; -5,5	-11,0; -10,1; -9,8; -9,1	5

Note. (●) indicates ¹³C labelled carbon atoms; (*) indicates that the NMR line assignment was confirmed in experiments with model compounds.

^a Chemical shifts reported in literature are given in brackets: (s) solution data (44), (g) gaseous phase data (45).

^b Other assignments of the corresponding lines are given in brackets.

^c Splitting was not determined if the intensity of the corresponding line was low, or if the line was significantly broadened. Splittings which are not identified unambiguously because of multiple patterns overlapping are given in brackets.

stream then passed over a vertical catalyst bed heated by a tubular furnace. Product gases were analyzed by on-line gas chromatography. A typical run consisted of loading about 300 mg of catalyst into the reactor and re-reducing the metal *in situ* with a flow of H₂ at 700 K for 2 h before introducing He and the reactant *n*-hexane. The steady state reaction was carried out for 0.5 h at 700 K before heating to the standard temperature of 750 K. The weight hour space velocity (WHSV) was 5.5 to 467 (s⁻¹ × g⁻¹ Pt/Pd × g hexane). Product gases were quantified by on-line gas chromatography and identified by gas chromatography coupled with mass spectrometer.

The selectivity for a specific reaction product was determined as percentage of a product in feed-free products.

RESULTS

In situ ¹³C MAS NMR

Effect of reactant loading. *n*-Hexane conversion depends to a great extent upon the experimental conditions: temperature, pressure, and contact time.

To make the reaction conditions compatible with those obtained in the continuous flow microreactor and to favor the observation of all the reaction intermediates, one should decrease contact time. In batch conditions, this can be achieved by increasing the reagent loadings. However, high loadings lead to an increase of pressure in the batch system. Simple estimates of the pressures (in Torr) in the NMR cells for different loadings at various temperatures are given below (the numbers are rounded):

Loadings (mg)	298 K	573 K	653 K
1	230	440	5300
4	930	1800	2000
12	2800	5400	6100

For these estimates, the adsorption is not taken into account and real pressures in the NMR cell are, of course, less due to adsorption. On the other hand, the chemical reactions which proceed at higher temperatures (dehydrogenation, cracking) may increase the number of moles in the gas phase leading to an increase of the total pressure in the cell. Therefore it should be taken into account that the above estimates are rather approximate. However, they clearly show that for high loadings (e.g., 12 mg/NMR cell) and at high temperatures, pressure is most probably higher than atmospheric. The increase of the pressure can cause explosion of the NMR cell, or can influence the adsorption and exchange processes (31, 40, 43) and the reaction equilibrium (40).

Thus, on one hand, increasing of hexane loadings is favorable because of the decreasing contact time. On the other hand, it is unfavorable because it can cause high

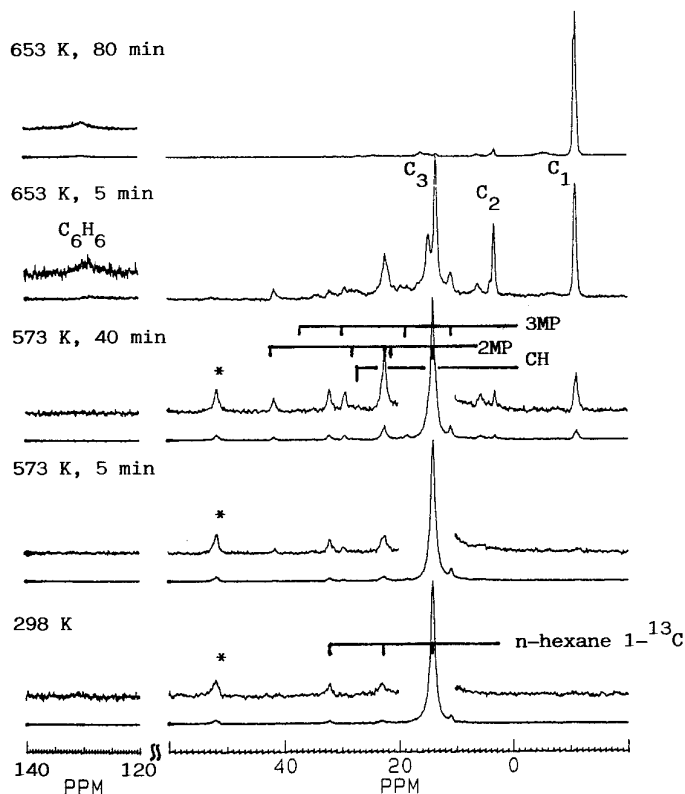


FIG. 2. ¹³C MAS NMR spectra observed before and after reaction of *n*-hexane 1-¹³C over Pt/KL at progressively increasing temperatures. Abbreviations used: 3MP, 3-methylpentane; 2MP, 2-methylpentane; MCP, methylcyclopentane; CH, cyclohexane; C₃, propane; C₂, ethane; C₁, methane. Asterisks denote spinning sidebands.

pressures in the batch. Our preliminary experiments (with 1, 4, and 12 mg) showed that 4 mg/NMR cell is the optimal loading for investigation of our system.

***n*-Hexane adsorption.** ¹³C MAS NMR spectra observed after adsorption of *n*-hexane 1-¹³C on Pt/Mg(Al)O (Fig. 1) and Pd/Mg(Al)O (Fig. 3) catalysts show an intense resonance at 13.8 ppm which corresponds to the labelled methyl group of *n*-hexane, and two weak resonances at ca. 23.2 and 32.3 ppm, attributed to natural-abundant methylene carbons, respectively (Table 1). The methyl resonance is not shifted much relative to *n*-hexane in solution (13.7 ppm) (44). On the contrary, resonance shifts of 0.4–0.5 ppm to lower fields are observed for methylene groups, due to their higher distortion upon adsorption (34).

The situation is, however, different for *n*-hexane on Pt/KL. In this case, methyl groups are more strongly affected upon adsorption than methylene groups (Table 1). This effect is probably due to end-on or terminal adsorption to the Pt surface in the unidimensional channels of zeolite L (9, 13).

In the case of Pt/KL, an additional line at 11 ppm is observed (Fig. 2). The assignment of this line was made

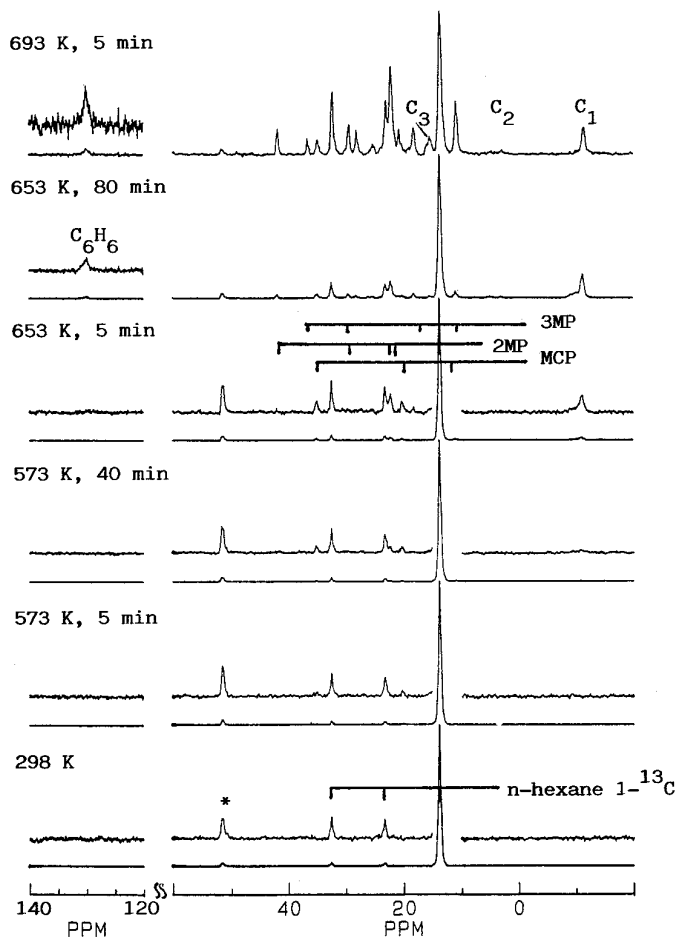


FIG. 3. ^{13}C MAS NMR spectra observed before and after reaction of *n*-hexane $1\text{-}^{13}\text{C}$ over Pd/Mg(Al)O at progressively increasing temperatures. Abbreviations used: 3MP, 3-methylpentane; 2MP, 2-methylpentane; MCP, methylcyclopentane; CH, cyclohexane; C_3 , propane; C_2 , ethane; C_1 , methane. Asterisk denotes spinning sidebands.

on the basis of variable temperature experiments, cross-polarization experiments, and non- ^1H decoupled spectra (Fig. 4). The line was characterized by the following features:

- The intensity of the line is affected by temperature (Figs. 4a–4c). It disappears at 253 K and increases at 373 K with respect to the resonance at 13.8 ppm.
- In the absence of ^1H decoupling, the resonance at 11 ppm is a quadruplet (Fig. 4d).
- $^1\text{H}\text{-}^{13}\text{C}$ cross-polarization is not observed for this line (Fig. 4e).

These observations indicate that the 11-ppm resonance line stems from gaseous *n*-hexane $1\text{-}^{13}\text{C}$ species. This hypothesis is supported by experiments at high loadings (12 mg) over Pt/Mg(Al)O, when the resonance at 11 ppm is also observed. Observation of gaseous species was also

reported for methanol and dimethylether (31, 46), and methane adsorbed on zeolites (34).

Identification of the main reaction products and intermediates. *n*-Hexane conversion was studied by heating the NMR cells at progressively increased temperatures for various periods of time. The same experimental protocol was used for all samples. The results are presented in Figs. 1–3.

In the case of Pt/Mg(Al)O, the reaction begins at 523 K (Fig. 1). A typical NMR spectrum observed after 5 min heating at 573 K shows a set of resonances in the chemical shift range of 11 to 50 ppm, which corresponds to isomers of *n*-hexane. Further heating at 573 K for another 40 min results in the appearance of the resonances in the chemical shift range of -11 to 25 ppm, which corresponds to the products of cracking. Finally, when temperature reaches 653 K, a broad resonance is detected at ca. 130 ppm, which corresponds to the formation of olefinic and/or aromatic compounds.

^{13}C MAS NMR spectra observed on Pt/KL and Pd/Mg(Al)O show the same groups of products. However, the following differences emerge: (1) On both of them, isomerization begins only at 573 K, being the slowest on Pd/Mg(Al)O (Fig. 2, 3). (2) In the case of Pd/Mg(Al)O, the NMR lines corresponding to the products of cracking appear only at 653 K (Fig. 3), while on Pt/KL cracking

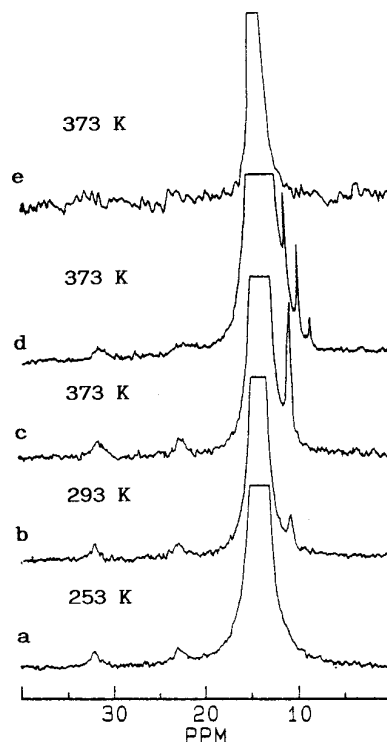


FIG. 4. ^{13}C MAS NMR spectra observed immediately after adsorption of *n*-hexane $1\text{-}^{13}\text{C}$ over Pt/KL: (a–c) ^1H -decoupled spectra recorded at different temperatures; (d) non- ^1H -decoupled spectrum; (e) CP spectrum.

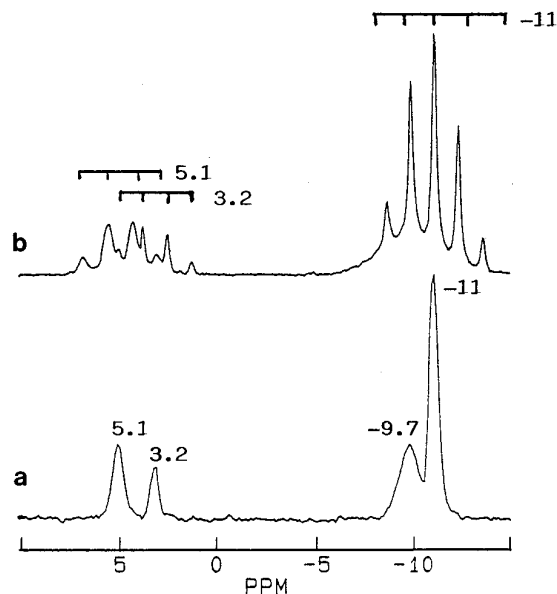


FIG. 5. Aliphatic regions of typical ^{13}C MAS NMR spectra observed after *n*-hexane $1\text{-}^{13}\text{C}$ reaction at 653 K over Pt/Mg(Al)O catalyst: (a) ^1H -decoupled spectrum; (b) non- ^1H -decoupled spectrum.

starts already at 573 K (Fig. 2), as is observed for Pt/Mg(Al)O (Fig. 1), the rate of cracking being the highest on Pt/KL.

The assignment of the individual lines observed in the spectra is based on the comparison of their chemical shifts with solution (44) and gaseous phase (45) data, and on the examination of multiplet patterns in the absence of proton decoupling. When a given signal could not be unambiguously assigned to a single molecular species using the above criteria, direct adsorption of the model compound was performed to confirm the assignment.

Table 1 lists the observed resonances, their splitting in non- ^1H -decoupled conditions, their assignments, and the corresponding chemical shifts (referred to TMS) in gaseous state and in solution.

The assignments of the lines corresponding to methyl groups of hexanes, pentanes, butanes, and propane are straightforward since their chemical shifts are close to those reported for solutions (Table 1). Moreover, in the absence of ^1H -decoupling, these lines are split into quadruplets with relative intensities 1:3:3:1, corresponding to methyl groups. However, some of these resonance lines may stem from a number of overlapping species which cannot be resolved because of the identity of their chemical shifts. Thus, the line at ca. 14 ppm may stem from *n*-hexane $1\text{-}^{13}\text{C}$, 2-methylpentane $5\text{-}^{13}\text{C}$, and *n*-pentane $1\text{-}^{13}\text{C}$. Similarly, the line at 11 ppm corresponds to two overlapping species from 3-methylpentane $1\text{-}^{13}\text{C}$ and 2-methylbutane $4\text{-}^{13}\text{C}$, respectively.

The lines assigned to CH_2 and CH groups of aliphatic products split into triplets and doublets, respectively, when

the measurements are performed in the absence of ^1H -decoupling (Table 1). In some of the cases, these resonances (especially, resonances corresponding to CH groups) show a significant shift to lower field with respect to solution data. Indeed, the geometry and electron distribution in these groups are expected to be more noticeably affected by adsorption. Similar observations were made for aliphatics adsorbed on H-ZSM-5 catalyst (34).

Light aliphatic products (ethane and methane) are characterized by two resonance lines, belonging to adsorbed and gaseous species (Table 1). The assignment of the ethane lines at 5.1 and 3.2 ppm to adsorbed and gaseous species, respectively, is based on the following arguments:

(1) In the absence of ^1H -decoupling, both resonances are split into quadruplets with relative intensities 1:3:3:1 and a characteristic $^{13}\text{C}\text{-}^1\text{H}$ coupling constant of 125 Hz (Fig. 5).

(2) The resonance at 3.2 ppm is close to that reported for gaseous ethane (44) and that at 5.1 is close to solution data for ethane (45).

(3) The line at 5.1 ppm is broader than that at 3.2 ppm (Fig. 5).

(4) The ratio of the line intensities is affected by temperature. The 5.1 ppm line is the only one observed below ambient temperature. The intensity of the 3.2-ppm line increases with temperature.

Similar arguments are used to assign the resonances at ca. -9.7 and -11 ppm to adsorbed and gaseous methane, respectively (Fig. 5).

The products of dehydrocyclization are characterized by three resonances at ca. 20, 27, and 35 ppm (Table 1). The resonances at 20.3 and 34.9 ppm are attributed to methylcyclopentane $\alpha\text{-}^{13}\text{C}$ and $1\text{-}^{13}\text{C}$, because of the following reasons. In the absence of ^1H -decoupling, these lines are split into a quadruplet and a triplet indicating that they correspond to a methyl and a methylene group, respectively. Moreover, they appear simultaneously and their intensities are similar at the beginning of the reaction. The assignments of these lines are further confirmed in an independent reference experiment with nonlabelled methylcyclopentane adsorbed on Pt/Mg(Al)O (Fig. 6a). The assignment of the resonance line at 27.4 ppm to cyclohexane is also checked and confirmed (Fig. 6b). At higher temperatures or contact times the resonance line at 34.9 ppm, corresponding to methylcyclopentane $1\text{-}^{13}\text{C}$, may overlap with those at 34.8 ppm assigned to *n*-pentane $1\text{-}^{13}\text{C}$ resulting from the consecutive isomerization and cracking of *n*-hexane (Table 1).

It is noteworthy that resonance lines corresponding to cyclic products are shifted to higher field upon adsorption, in contrast to aliphatic carbon lines, which are shifted down-field, probably because of their specific adsorption modes on the surface.

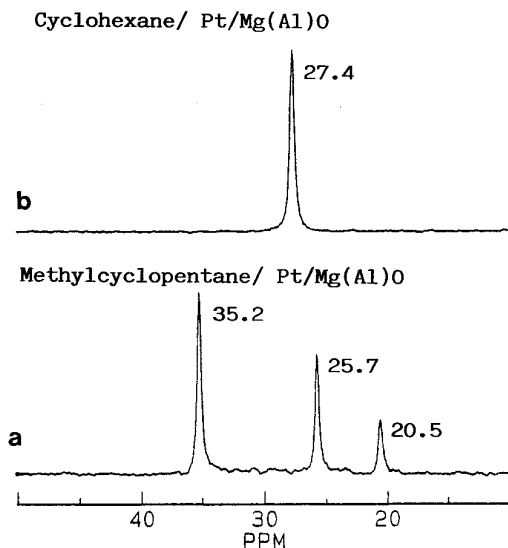


FIG. 6. ^{13}C MAS NMR spectra observed immediately after adsorption of methylcyclopentane (a) and cyclohexane (b) over Pt/Mg(Al)O catalyst.

The broad line at ca. 130 ppm may be attributed to several carbons in different olefinic and aromatic compounds: (E)-2-hexene 3- ^{13}C (131.7 ppm), (Z)-2-hexene 3- ^{13}C (130.8 ppm), (E)-3-hexene 3- ^{13}C (131.2 ppm), (Z)-3-hexene 3- ^{13}C (131.2 ppm), cyclopentene (130.8 ppm), cyclohexene (127.4 ppm), and benzene (128.5 ppm). Spectra recorded in the absence of ^1H -decoupling do not help in assigning the 130 ppm resonance because of line broadening. To verify whether this line can correspond to hexenes, a mixture of hexene isomers was adsorbed onto Pt/Mg(Al)O and the ^{13}C MAS NMR spectrum of this sample was compared to those observed after reaction of *n*-hexane at 653 K, as shown in Fig. 7. A significant difference in chemical shifts and line widths of the resonances ob-

served in the spectra suggest that the line at 130 ppm could hardly be attributed to hexenes. Moreover, ^1H MAS NMR spectra do not show any resonances which can be assigned to olefinic protons of hexenes (5–5.7 ppm) or cycloalkenes (5.6 ppm). On the contrary, the line corresponding to the protons of benzene (7.6 ppm) is well observed (Fig. 8).

All these observations indicate that the 130 ppm line should be assigned to benzene. The olefinic and aliphatic carbons of hexenes and cycloalkenes are not observed under our experimental conditions.

The resonance lines corresponding to alkylaromatics were observed only on Pd/Mg(Al)O catalyst (Table 1, Fig. 9). The assignment of the lines at 125 and 139 ppm to alkylaromatics is based on the following observations (Fig. 9):

- (1) These resonances appear at high conversion.
- (2) They are too broad to be attributed to hexenes and other olefins. Indeed, it was shown in independent experiments that olefins adsorbed on these catalysts give narrower lines (Fig. 7).
- (3) Their chemical shifts correspond to those reported for aromatic carbons in alkylaromatics (Table 1).

The lines at ca. 20.4 and 28.2 ppm are characterized by several features (Fig. 9):

- (1) They appear simultaneously with those at 125 and 139 ppm.
- (2) Their chemical shifts correspond to those reported for methyl and ethyl carbons in mono- and polysubstituted aromatics (Table 1).
- (3) They do not disappear at longer reaction times when all C_6 - C_5 hydrocarbons are cracked into light alkanes (methane, ethane, and propane).
- (4) These lines are broader relative to all the other resonances observed in the aliphatic region of the spectra.

Although the lines at ca. 20.4, 28.2, 125, and 137 ppm

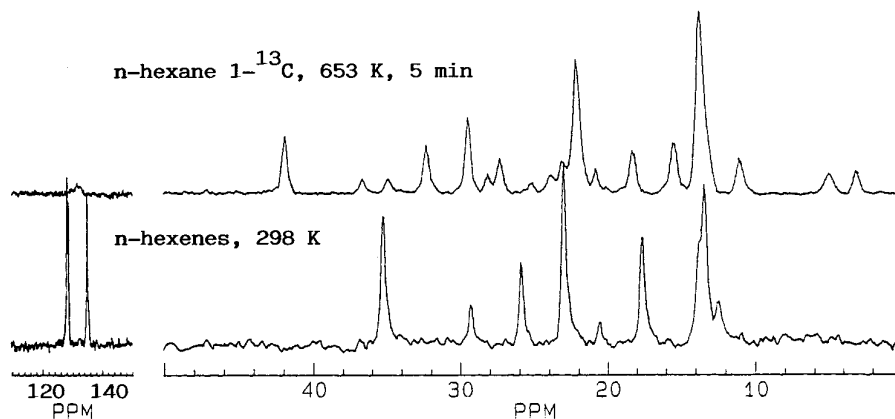


FIG. 7. Comparison of the ^{13}C MAS NMR spectra observed over Pt/Mg(Al)O after 5 min reaction of *n*-hexane at 653 K and after adsorption of a mixture of *n*-hexene isomers (1-hexene, (E and Z)-2-hexenes, (E and Z)-3-hexenes).

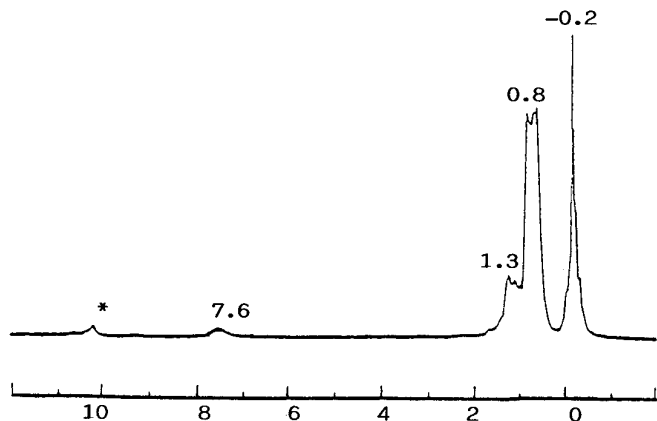


FIG. 8. ^1H MAS NMR spectra observed after 80 min reaction of *n*-hexane $1\text{-}^{13}\text{C}$ over Pt/Mg(Al)O at 653 K. Asterisk denotes spinning sideband.

cannot be assigned unambiguously to individual products because they most probably stem from different overlapping species, all the above observations indicate that they correspond to methyl- and ethyl-substituted benzenes.

The comparison of the ^{13}C MAS NMR spectra observed in course of *n*-hexane reaction over different catalysts, and of the individual resonances assignments (Figs. 1 to 3 and Table 1) reveal the following differences in reaction products and their mobilities:

- The resonance lines are in general broader on Pt/KL than on Pt/Mg(Al)O and Pd/Mg(Al)O, due to restricted mobility of the adsorbed species within the zeolite channels.
- The resonances corresponding to methyl groups of

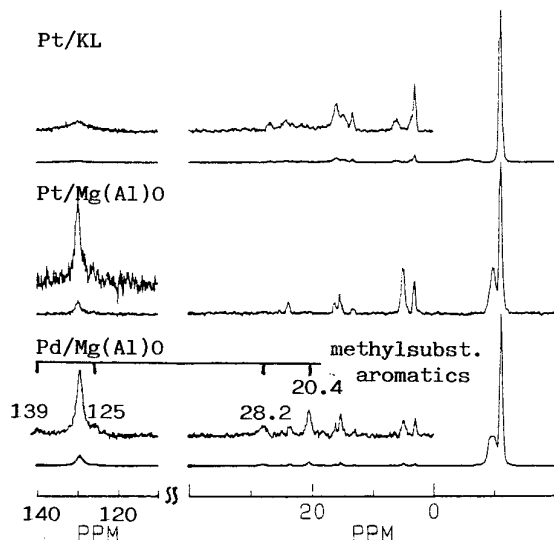


FIG. 9. ^{13}C MAS NMR spectra observed after reaction of *n*-hexane $1\text{-}^{13}\text{C}$ over Pt/Mg(Al)O, Pt/KL, and Pd/Mg(Al)O catalysts at 653 K.

hexanes and pentanes Pt/KL are shifted down-field with respect to those observed on Pt/Mg(Al)O and Pd/Mg(Al)O. This observation is in line with end-on adsorption of these molecules on metal particles in the unidimensional channels of zeolite L (9, 13).

- No methylcyclopentane formation is observed over Pt/KL catalyst, indicating preferential 1/6 ring closure. This observation agrees with the molecular die hypothesis (9, 13) and the confinement model (10).

- In contrast, no cyclohexane was observed over Pd/Mg(Al)O, indicating preferential 1/5 ring closure on this catalyst.

- Another new observation is the formation of methyl- and ethyl-substituted aromatics only on Pd/Mg(Al)O catalyst.

Quantification of the NMR data. For the quantitative comparison of the reaction kinetics and selectivity over different catalysts two separate sets of experiments were carried out on each catalyst. In these experimental sets, the reaction temperature was fixed and the NMR spectra were acquired as a function of reaction time. Two reaction temperatures were selected: 573 K, chosen as an optimal temperature for *n*-hexane isomerization and dehydrocyclization, and 653 K, chosen as a temperature required for aromatization and cracking. The NMR line intensities were then determined in each run and *n*-hexane conversions, product yields, and selectivities were calculated, as defined in the Experimental section. The kinetics of *n*-hexane transformation and selectivities towards different groups of products on Pt/Mg(Al)O, Pt/KL, and Pd/Mg(Al)O catalysts are compared in Figs. 10 and 11, respectively.

The quantification of the NMR data is the basis for the comparison of the *in situ* NMR results with those obtained in continuous flow microreactor experiments.

Continuous Flow Microreactor Experiments

Conversion in flow experiments was varied by changing weight hour space velocities. To do this, 5 or 6 runs at WHSV in the range of 5.5 to 467 ($\text{s}^{-1} \times \text{g}^{-1} \text{Pt/Pd} \times \text{g hexane}$) were performed at 750 K on each catalyst. The *n*-hexane conversions obtained in different runs were plotted as a function of contact time and are compared for various catalysts in Fig. 12.

Reaction products were subdivided into five groups as denoted below:

- isomerization products, all isomers of hexane;
- hydrocracking products, all hydrocarbons with a number of carbon atoms less than 6, including olefins and cyclic products;
- dehydrocyclization products, C_6 cycloalkanes and cycloalkenes;
- dehydrogenation products, hexenes and hexadienes;

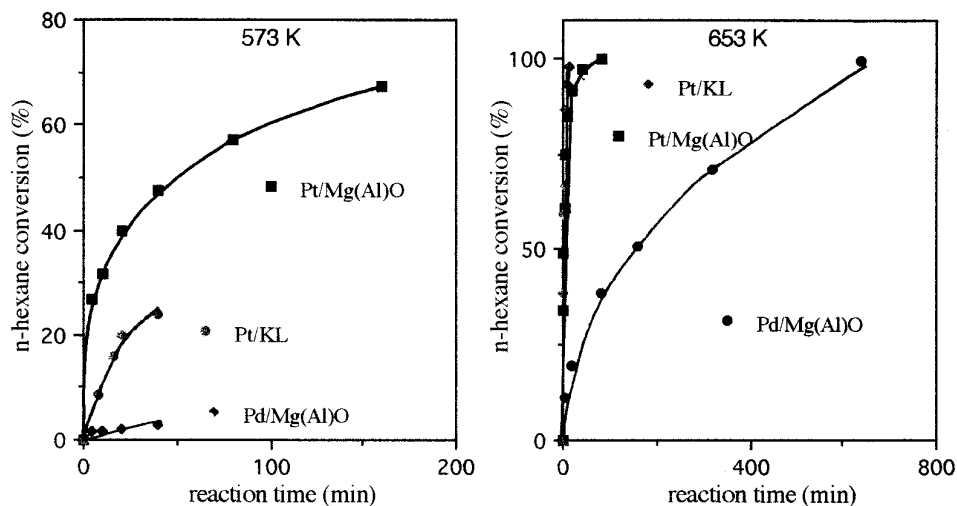


FIG. 10. Variation of *n*-hexane $1\text{-}^{13}\text{C}$ conversion as a function of reaction time. *In situ* ^{13}C MAS NMR experiments.

(V) aromatization products, benzene and alkylsubstituted aromatics.

The selectivities to different groups of products were determined in each run and plotted versus conversion as was done in the case of NMR experiments (Fig. 11).

It should be mentioned that the continuous flow reactor results are presented in this paper only for comparison with *in situ* NMR results. A more detailed description of the catalytic performance of Pt/Mg(Al)O, Pt/KL, and Pd/Mg(Al)O in *n*-hexane reforming is given elsewhere (15–18).

DISCUSSION

The experiments carried out in batch/NMR conditions at 573 K (Fig. 10) indicate that *n*-hexane conversion increases in the following order of catalysts: Pd/Mg(Al)O < Pt/KL < Pt/Mg(Al)O, while at 653 K the activity of Pt/KL becomes higher than that of Pt/Mg(Al)O. The same activity sequence was observed in flow/GC conditions at 750 K (Fig. 12), indicating that the catalysts operate in a similar way in batch/NMR and flow/GC systems. However, the maximum conversions reached in a flow reactor are much lower than those obtained in batch conditions even when reaction in a flow system was performed at much higher temperatures. This can be due to the longer contact times achieved in the batch/NMR system.

The product distributions observed in flow and NMR experiments are compared in Table 2 and Fig. 11. The following differences emerge:

- Neither linear nor branched hexenes were observed in NMR experiments. In contrast, they are the main products at low conversions in the flow reactor studies.

- Selectivity to benzene is much higher in flow conditions at all conversion levels.

- Olefinic products of cracking and dehydrocyclization are not detected in batch conditions.

- 2, 2-methylbutane was observed only in NMR experiments.

The most noticeable discrepancy is the absence of hexenes. Three possible reasons are: hexenes are not detected, are transformed rapidly into other products, or are not formed at all in the NMR experimental conditions.

It was shown above that the resonances corresponding to hexenes are not broadened beyond the detection limit, nor are they in overlap with those of other products. A ^{13}C carbon balance revealed that no ^{13}C intensity loss occurs at conversion levels up to 90%. ^1H MAS NMR experiments confirm the absence of hexenes (Fig. 8).

It has been proposed that in batch/NMR conditions olefins are unstable with respect to self-hydrogenation (47, 48), aromatization (34, 36, 40), or coke formation (39, 49) over various metal supported and zeolite catalysts. The reactivity of linear hexenes over Pt/Mg(Al)O was checked at 573 and 653 K, respectively (Fig. 13). Hexenes were found to be rather stable at 573 K. After 10 min heating, conversion of hexenes was not higher than 20%. However, when the temperature was increased up to 653 K hexenes were rapidly converted into benzene and *n*-hexane.

This result indicates that formation of hexenes followed by their rapid transformation into benzene may occur under our experimental conditions. However, this suggestion is questioned by the following observations:

- (1) No resonance corresponding to benzene and no ^{13}C intensity loss due to coke formation are observed at 573 K, indicating that hexene intermediates were probably not formed in large amounts at this temperature.

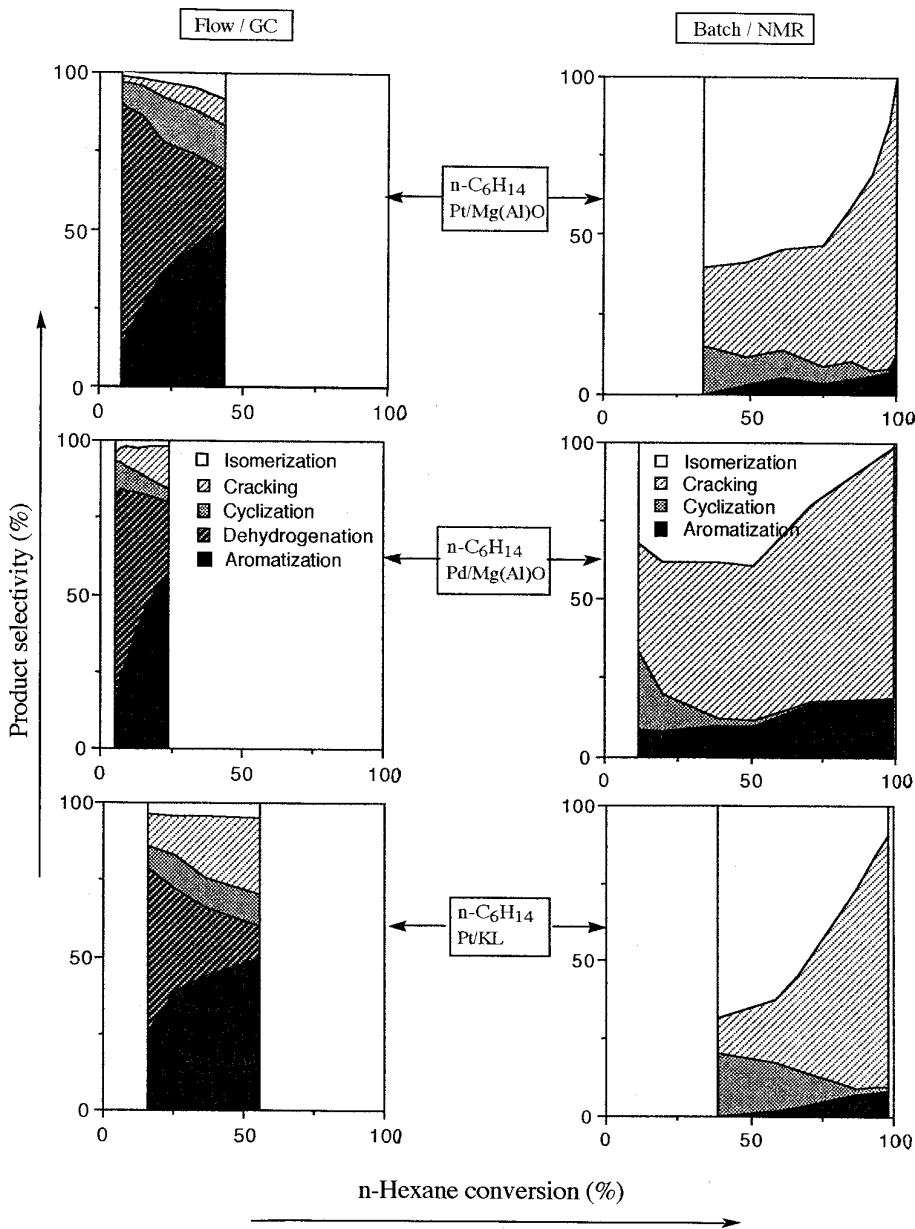


FIG. 11. Comparison of the selectivity diagrams observed for *n*-hexane conversion over Pt/Mg(Al)O, Pt/KL, and Pd/Mg(Al)O catalysts in batch/NMR (653 K) and flow/GC (750 K) experiments. The width of the band measures selectivity to the indicated reaction pathway as a function of conversion.

(2) Selectivity to benzene at 653 K was an order of magnitude lower relative to that observed in a flow reactor (Fig. 11), indicating that aromatization via partially dehydrogenated linear intermediates claimed for flow conditions (50) is suppressed in batch/NMR conditions.

All these observations lead to the conclusion that *n*-hexenes are not formed as products to any appreciable extent under the NMR experimental conditions. High pressures induced in the NMR cells at high temperature may

shift the reaction equilibrium (40), thereby favoring bimolecular hydrogenation with respect to dehydrogenation, leading to a different product distribution.

As the *n*-hexane dehydrogenation route is prevented in batch/NMR conditions, there must be another pathway leading to benzene formation. It is most probably conventional 1–6 dehydrocyclization, as reported for supported metal catalysts (2, 51). This suggestion is based on the observation of significant concentrations of cyclic hydrocarbons at low and intermediate conversions of *n*-hexane

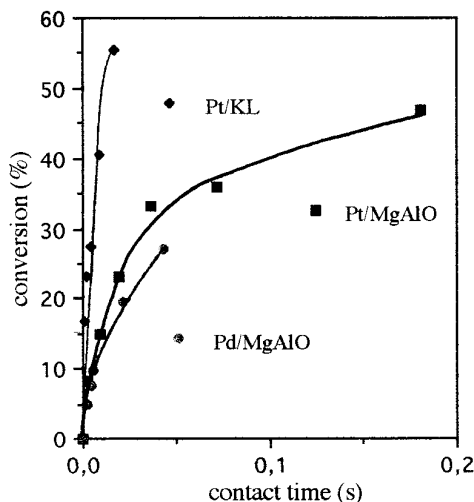


FIG. 12. Variation of *n*-hexane 1-¹³C conversion as a function of reaction time at 750 K. Continuous flow microreactor/GC experiments.

(Table 2) and on the monotonic decrease of cyclic hydrocarbon yields with increasing benzene yields (Fig. 11).

Since on Pd catalyst only 1–5 ring closure was observed, we propose that, in this case, aromatization proceeds via a methylcyclopentane intermediate. Ring enlargement of methylcyclopentane to form benzene has been described by Amir-Ebrahimi *et al.* (52).

It is noteworthy that this route can also operate in flow conditions, as cyclic intermediates were also identified in that case (Table 2).

The absence of olefinic products of cracking and dehydrocyclization in the course of *n*-hexane conversion may

TABLE 2

Comparison of *n*-Hexane Conversion Products Obtained in Experiments Using *in situ* ¹³C MAS NMR and Continuous Flow Microreactor/GC Techniques

Product group	Batch/NMR: 653 K	Flow/GC: 750 K
Isomerization	2-Methylpentane 3-Methylpentane 2,2-Dimethylbutane	2-Methylpentane 3-Methylpentane
Hydrocracking and cracking	Methane Ethane Propane Butanes Pentanes Cyclopentane	Methane Ethane, ethylene Propane, propene Butanes, butenes Pentanes, pentenes Cyclopentane, cyclopentene
Dehydrocyclization	Methylcyclopentane Cyclohexane	Methylcyclopentane Cyclohexene, Cyclohexadiene
Dehydrogenation	—	Linear and branched hexenes
Aromatization	Benzene Methyl and ethyl substituted Benzene	Benzene

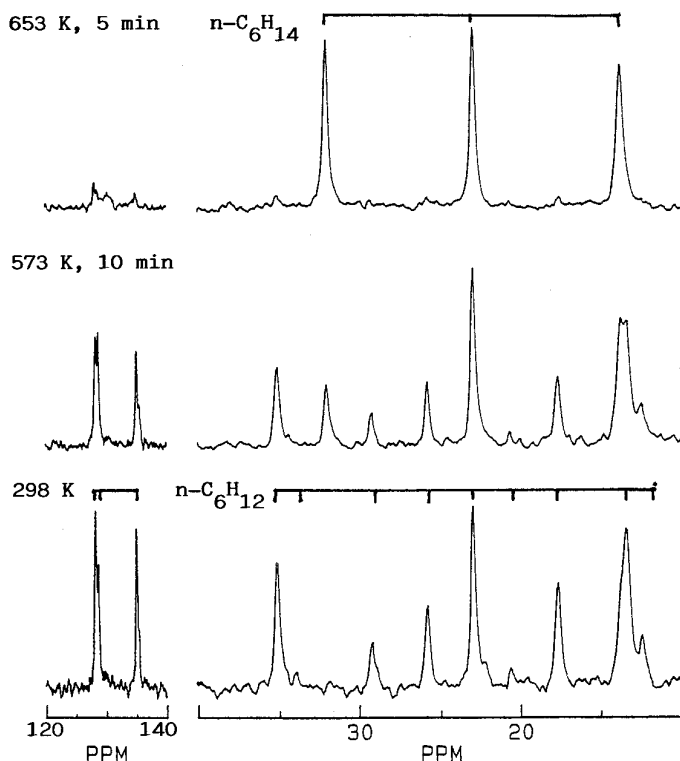


FIG. 13. ¹³C MAS NMR spectra observed before and after reaction of linear hexenes (1-hexene, (E and Z)-2-hexenes, (E and Z)-3-hexenes) over Pt/Mg(Al)O at 573 and 653 K.

also be due to rapid hydrogenation in batch conditions. However, the source of hydrogen must be identified in this case.

A simple hydrogen balance for *n*-hexane conversion is presented in Table 3. One hydrogen molecule is required (at least formally) for each carbon–carbon bond that is cracked to form two noncyclic alkane molecules. The amount of hydrogen consumed corresponds to *n*-hexane conversion into cracking products (Y_{cr}). The release of hydrogen occurs in the course of dehydrocyclization, aromatization, and graphitic coke formation. Dehydrocyclization releases one hydrogen molecule, aromatization yields 4 H₂, and 7 H₂ are formed from one *n*-hexane molecule in the course of coke formation. Hydrogen consumption in hydrocracking is further compared with hydrogen release during dehydrocyclization and aromatization over different catalysts as shown in Fig. 14.

It appears that, on Pd/Mg(Al)O, dehydrocyclization and aromatization sources of hydrogen are sufficient for hydrocracking. In contrast, in the case of Pt-containing catalysts, hydrogen consumption is twice as much as the hydrogen release in dehydrocyclization and aromatization. Therefore we conclude that coke is formed on the Pt catalysts during *n*-hexane conversion. A simple estimation shows that about 5–6% of *n*-hexane may end up in graphitic coke

TABLE 3
Hydrogen Balance for *n*-Hexane Conversion in Batch/NMR Systems

H ₂ consumed		H ₂ released	
Reaction	H ₂ concentration ^a	Reaction	H ₂ concentration ^a
Cracking $C_6H_{14} + H_2 \rightarrow 2 C_nH_{2n+2}$	Y_{cr}	Dehydrocyclisation $C_6H_{14} + H_2 \rightarrow C_6H_{12} + H_2$	Y_{cycl}
		Aromatisation $C_6H_{14} \rightarrow C_6H_6 + 4 H_2$	$4 Y_{ar}$
		Coking $C_6H_{14} \rightarrow 6 C + 7 H_2$	$7 Y_{coke}$

^a Y_{cr} , yield of cracking products; Y_{cycl} , yield of cyclic hydrocarbons; Y_{ar} , yield of aromatic products; Y_{coke} , yield of coke.

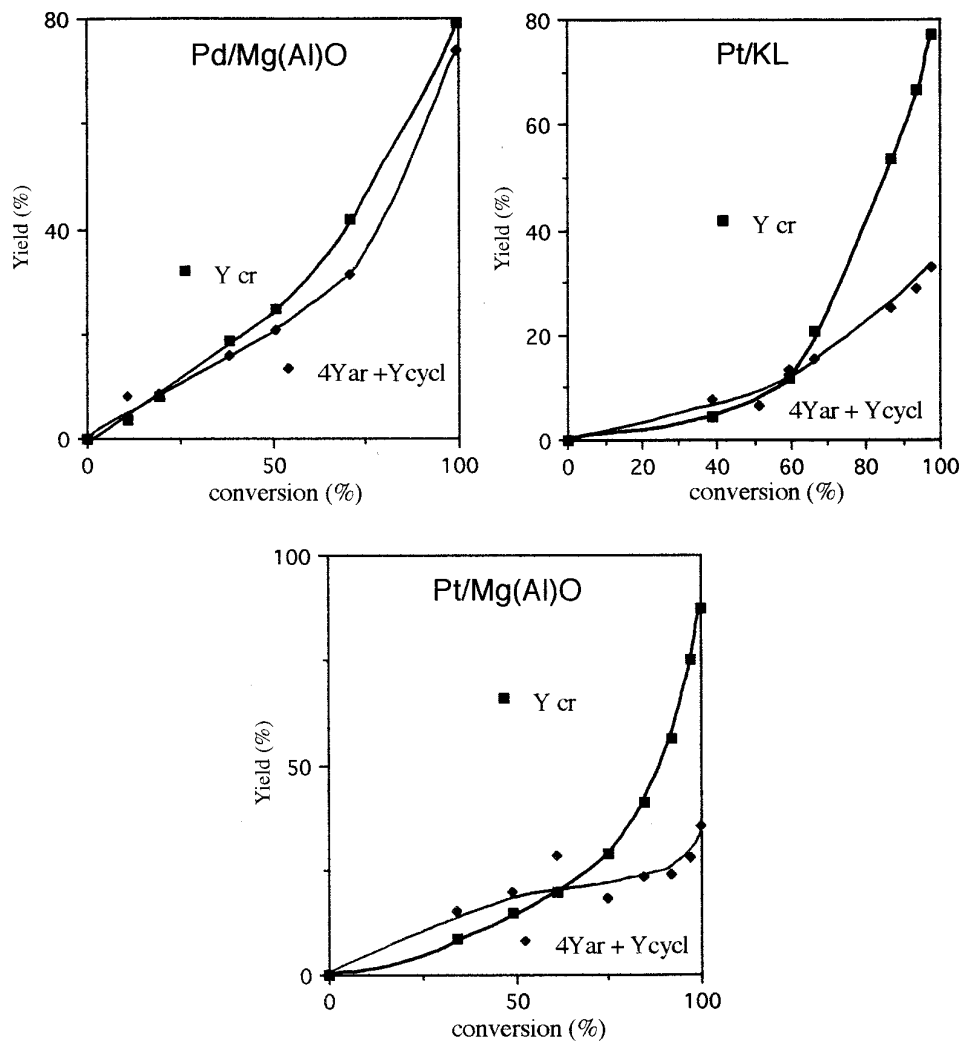


FIG. 14. Variations of hydrogen release during aromatization and dehydrocyclization ($4Y_{ar} + Y_{cycl}$) and hydrogen consumption during hydrocracking (Y_{cr}) as a function of *n*-hexane conversion.

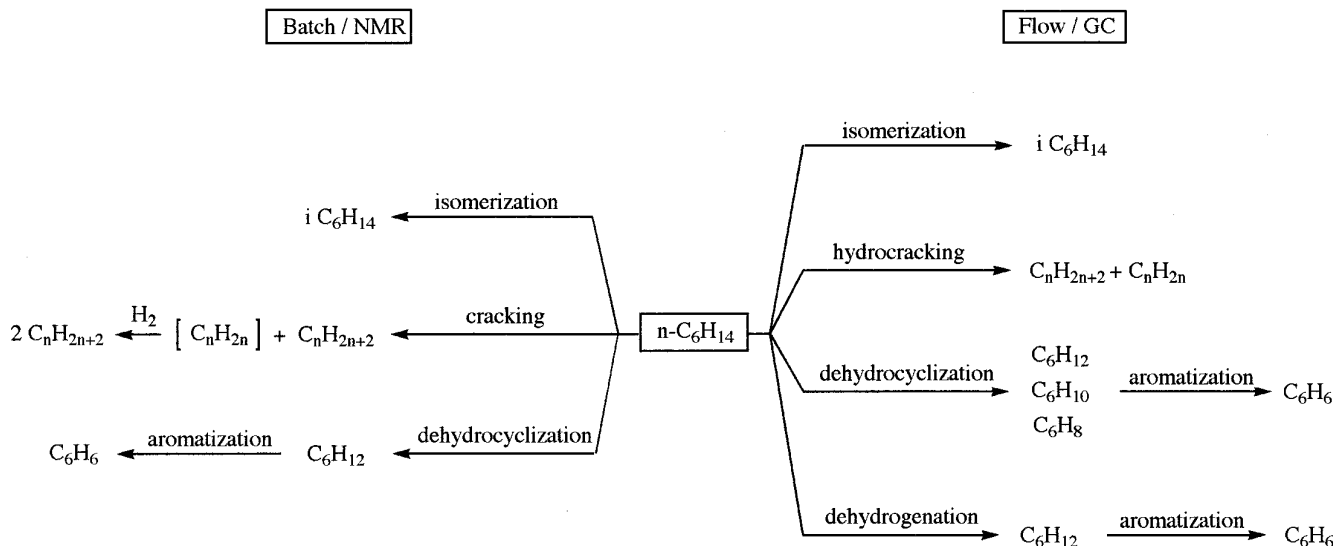


FIG. 15. Comparison of the main reaction pathways operating in flow/GC and batch/NMR conditions.

at high conversion. On Pd catalysts, no coke is formed according to our estimations.

n-Hexane isomerization does not reveal significant differences for batch and flow conditions. 2-Methylpentane and 3-methylpentane are the major products in both experiments. Traces of 2, 2-methylbutane observed in batch/NMR is probably due to longer contact times favoring secondary isomerization.

The reaction network schematized in Fig. 15 rationalizes all the above observations. In continuous flow microreactor/GC experiments *n*-hexane is converted via 4 parallel pathways: isomerization, cracking, dehydrocyclization, and dehydrogenation. Dehydrocyclization and dehydrogenation routes lead further to benzene as a final product. The contribution of the former to aromatization is lower with respect to the latter. In the NMR batch experiments the dehydrogenation pathway is prevented. The olefinic products of cracking are rapidly hydrogenated to alkanes. Benzene is formed via dehydrocyclization only.

In both experimental conditions the aromatization selectivity is enhanced in the presence of Pd. The highest isomerization activity is observed on Pt/Mg(Al)O · Pt/KL catalyst leads to terminal cracking enhancement with respect to isomerization.

We have demonstrated for three different catalysts that isomerization, cracking, and dehydrocyclization pathways of *n*-hexane reforming can be monitored *in situ* using solid-state NMR techniques, while the dehydrogenation pathway is prevented under NMR/batch conditions. The identification of the reaction products and intermediates made in this paper will be the basis for detailed mechanistic study to be presented in our further contributions (53, 54).

CONCLUSIONS

It has been found that the reaction network of *n*-hexane conversion over Pt/Mg(Al)O, Pd/Mg(Al)O, and Pt/KL catalysts consists of four parallel pathways: isomerization, cracking, dehydrocyclization, and dehydrogenation. Dehydrocyclization and dehydrogenation routes lead to benzene as a final product. In the continuous flow microreactor experiments, dehydrogenation followed by aromatization is the main reaction pathway. On the contrary, under the NMR/batch conditions, dehydrogenation is prevented, and isomerization and cracking become the major reaction routes. The products of isomerization, dehydrocyclization, and cracking do not reveal significant differences for continuous flow and NMR experiments, the only exception being that the olefinic products expected in cracking and dehydrocyclization are hydrogenated to alkanes and cycloalkanes in the latter case.

From this study it becomes apparent that isomerization, cracking, and dehydrocyclization pathways of *n*-hexane reforming can be monitored *in situ* using solid-state NMR techniques.

ACKNOWLEDGMENTS

I.I. Ivanova thanks the Belgian Program on Interuniversity Attraction Poles (PAI), Haldor Topsøe A/S, and the Laboratoire de Catalyse (FUNDP) for a research postdoctoral position. The authors thank G. Daelen for technical assistance and Johnson-Matthey Ltd. for supplying Pt salts.

REFERENCES

1. Tamm, P. W., Mohr, D. H., and Wilson, C. R., *Stud. Surf. Sci. Catal.* **38**, 335 (1988).

2. Gates, B. C., Katzer, J. R., and Schuit, G. C. A., "Chemistry of Catalytic Processes." McGraw-Hill, New York, 1979.
3. Ciapetta, F. G., and Wallace D. N., *Catal. Rev.* **5**, 67 (1972).
4. Sinfelt, J. H., *Catal. Sci. Tech.* **1**, 257 (1981).
5. Marin, G. B., and Froment, G. F., *Chem. Eng. Sci.* **37**, 759 (1982).
6. Bernard, J. R., in "Proceedings 5th International Zeolite Conference" (L. V. Rees, Ed.), p. 686. Heyden, London, 1980.
7. Hughes, T. R., Buss, W. C., Tamm, P. W., and Jacobson, R. L., *Stud. Surf. Sci. Catal.* **28**, 725 (1986).
8. Besoukhanova, C., Guidot, J., Barthomeuf, D., Breyse, M., and Bernard, J. R., *J. Chem. Soc. Faraday Trans. I* **77**, 1595 (1981).
9. Tauster, S. J., and Steger, J. J., *Mater. Res. Soc. Proc.* **111**, 419 (1988).
10. Derouane, E. G., and Vanderveken, D., *Appl. Catal.* **45**, L15 (1988).
11. Larsen, G., and Haller, G. L., *Catal. Lett.* **3**, 103 (1989).
12. Manninger, I., Lu, X. L., Tétényi, P., and Paál Z., *Appl. Catal.* **51**, L7 (1989).
13. Tauster, S. J., and Steger, J. J., *J. Catal.* **125**, 387 (1990).
14. Lane, G. S., Modica F. S., and Miller, J. T., *J. Catal.* **129**, 145 (1991).
15. Davis, R. J., and Derouane, E. G., *Nature (London)* **349**, 313 (1991).
16. Davis, R. J., and Derouane, E. G., *J. Catal.* **132**, 269 (1991).
17. Derouane, E. G., Jullien-Lardot, V., Davis, R. J., Blom, N. and Højlund-Nielsen, P. E., *Stud. Surf. Sci. Catal.* **75**, 1031 (1993).
18. Derouane, E. G., Jullien-Lardot, V., Pasau-Claerbout, A., Blom, N. J. and Højlund-Nielsen, P. E., North American Catalysis Society Meeting, 1993.
19. Tennison, S. R., Forster, A. I., McCarroll, J. J., and Joyner, R. W., in "ACS Petroleum Division Preprints, Seattle Meeting, March 20–25, 1983."
20. McCarroll, J. J., *Surf. Sci.* **53**, 297 (1975).
21. Clarke, J. K. A., Bradley, M. J., Garvie, L. A. J., Craven, A. J., and Baird T., *J. Catal.* **143**, 122 (1993).
22. Goldwasser, J., Bolivar, C., Ramon Ruiz, C., Arenas, B., Wanke, S. E., Royo, H., Barrios, R., and Giron, J., "Proceedings 8th, International Congress on Catalysis, Berlin, 1984," Vol. 5, p. 195. Dechema, Frankfurt-am-Main, 1984.
23. Paál, Z., Groeneweg, H., and Paál-Lukacs, J., *J. Chem. Soc. Faraday Trans.* **86**, 3159 (1990).
24. Garin, F., Aeiayach, S., Legaré, P., and Maire, G., *J. Catal.* **77**, 323 (1982).
25. Davis, S. M., Zaera, F., and Somorjai, G. A., *J. Catal.* **85**, 206 (1984).
26. Zaera, F., Godbey, D., and Somorjai, G. A., *J. Catal.* **101**, 73 (1986).
27. Dauscher, A., Garin, F., and Maire, G., *J. Catal.* **105**, 233 (1987).
28. Anderson, M. W., and Klinowski, J., *Nature* **339**, 200 (1989).
29. Haw, J. F., Richardson, B. R., Oshiro, I. S., Lazo, N. D. and Speed, J. A., *J. Am. Chem. Soc.* **111**, 2052 (1989).
30. Haw, J. K., *Spec. Publ. Roy Soc. Chem.* **114**, 1 (1992).
31. Anderson, M. W., and Klinowski, J., *J. Am. Chem. Soc.* **112**, 10 (1990).
32. Stepanov, A. G., Zamaraev, K. I. and Thomas, J. M., *Catal. Lett.* **13**, 407 (1992).
33. Ivanova, I. I., Brunel, D., Daelen, G., Nagy, J. B., and Derouane, E. G., *Stud. Surf. Sci. Catal.* **78**, 587 (1993).
34. Derouane, E. G., Abdul Hamid, S. B., Ivanova, I. I., Blom, N. and Højlund-Nielsen, P.-E., *J. Mol. Cat.* **86**, 371 (1994); see also Abdul Hamid, S. B., Dr.Sc. Thesis, University of Namur, Belgium, 1993.
35. Zilm, K. W., Bonneviot, L., Hamilton, D. M., Webb, G. G., and Haller, G. L., *J. Phys. Chem.* **94**, 1463 (1990).
36. Lambregts, M. J., Munson, E. J., Kheir, A. A., and Haw, J. F., *J. Am. Chem. Soc.* **114**, 6875 (1992).
37. Munson, E. J., Ferguson, D. B., Kheir, A. A., Lazo, N. D. and Haw, J. F., *J. Catal.* **136**, 504 (1992).
38. Nowak, A. K., Wilson, A. E., Roberts, K., and Datema, K. P., *J. Catal.* **144**, 495 (1993).
39. White, J. L., Lazo, N. D., Richardson, B. R. and Haw, J. F., *J. Catal.* **125**, 260 (1990).
40. Ivanova, I. I., Blom, N., Abdul Hamid, S. B., and Derouane, E. G. *Rec. Trav. Chim. Pays-Bas*, **113**, 454 (1994).
41. Schaper, H., Berg-Slot, J. J., and Stork, W. H. J., *Appl. Catal.* **54**, 79 (1989).
42. O'Rear, D. J., Loffler, D. G., and Boudart, M., *J. Catal.* **121**, 131 (1990).
43. Michael, A., Meiler, W., Michel, D., Pfeifer, H., Hoppach, D., and Delmau, J. *J. Chem. Soc. Faraday Trans. I* **82**, 3053 (1986).
44. E. Breitmaier, E., and Voelter, W. "Carbon-13 NMR Spectroscopy," VCH, Weinheim, 1987.
45. Nagy, J. B., Engelhardt, G., and Michel, D. *Adv. Colloid Interface Sci.* **23**, 67 (1985).
46. Oliver, F. G., Munson, E. J., and Haw, J. F., *J. Phys. Chem.* **96**, 8106 (1992).
47. Pruski, M., Kelzenberg, J. C., Gerstein, B. C., and King, T. S., *J. Am. Chem. Soc.* **112**, 4232 (1990).
48. Kye, Y. S., Wu, S. X., and Apple, T. M., *J. Phys. Chem.* **96**, 2632 (1992).
49. Wang, P. K., Slichter, C. P., and Sinfelt, J. H., *J. Phys. Chem.* **89**, 3606 (1985).
50. Lafyatis, D. S., Froment, G. F., Pasau-Claerbout, A., and Derouane, E. G., *J. Catal.*, **197**, 552 (1994).
51. Gault, F. G., "Mechanisms of Skeletal Isomerization of Hydrocarbons on Metals," Academic Press, New York, 1981.
52. Amir-Ebrahimi, V., Choplin, A., Parayre, P., Gault, F. G., *Nouv. J. Chim.* **4**, 431 (1980).
53. Ivanova I. I., Seivert, M., Pasau-Claerbout, A., Blom, N., and Derouane, E. G., to be published.
54. Ivanova I. I., Pasau-Claerbout, A., Blom, N., and Derouane, E. G., to be published.